BMC Biology

RESEARCH

Open Access

Juvenile hormone and BMP signaling modulate fat body cell fate during the transition of previtellogenic development to vitellogenesis

Zhongxia Wu[1], Wenxiao Zhao[1], Mengyao Lang[1], Qiongjie He[1], Yiying Li[1], Yuanyuan Hu[1], Yan Liu[1], Siqian Zheng[1], Huanhuan Shi[1] and Shutang Zhou[1*]

Abstract

Background Insect fat body, a central tissue for nutrient storage, energy metabolism, and protein synthesis, degrades by apoptosis and autophagy during larval metamorphosis. After adult emergence, the fat body grows rapidly with cell proliferation and polyploidization during the previtellogenic period but ceases cell proliferation in the vitellogenic phase. So far, the regulatory mechanisms underlying fat body cell fate decisions in adulthood remain unknown.

Results Transcriptomic analysis of locust fat body revealed the enrichment of pathways associated with cell cycle, nuclear division, and DNA replication. *Decapentaplegic* (*Dpp*) was among the top of differentially expressed genes in the signaling cascades involved in regulating cell proliferation. Abundance of Dpp, phosphorylated Mad (p-Mad), and Medea increased during the previtellogenic stage and subsequently declined in the vitellogenic phase. Knockdown of *Dpp*, *Mad*, and *Medea* resulted in suppressed fat body cell proliferation, along with remarkably reduced cell number and blocked *vitellogenin* (*Vg*) expression in the fat body as well as consequent arrest of egg development. Mad/Medea complex bound to the promoters of *cyclin B* (*CycB*) and *polo-like kinase 1* (*Plk1*) and stimulated their expression. Depletion of *CycB* and *Plk1* caused the defective phenotypes resembling *Dpp*, *Mad*, and *Medea* knockdown. In the vitellogenic phase, the high levels of juvenile hormone (JH) promoted the degradation of Medea via fizzy-related protein (Fzr)-mediated ubiquitination, leading to inhibited cell proliferation. The results suggest that fat body cell proliferation in the previtellogenic development is promoted by the bone morphogenetic protein (BMP) signaling pathway, whereas high levels of JH in the vitellogenic stage antagonize BMP signaling for ceasing cell proliferation.

Conclusions The findings provide novel insights into the regulation of fat body cell fate during the transition of previtellogenic growth to vitellogenic Vg synthesis for reproductive requirements.

Keywords BMP signaling, Juvenile hormone, Fat body, Cell proliferation, Female reproduction

Background

Insects have evolved intricated regulatory mechanisms to control essential life processes, including metamorphosis and reproduction. The fat body plays a pivotal role in these processes, serving as the primary site for vitellogenesis [1–3]. During the juvenile stage, the fat body expands and accumulates nutrients necessary for metamorphosis [1]. As insects transition into adulthood, the fat body

*Correspondence:
Shutang Zhou
szhou@henu.edu.cn
[1] State Key Laboratory of Cotton Bio-Breeding and Integrated Utilization, School of Life Sciences, Henan University, Kaifeng, China

undergoes significant structural and functional remodeling, shifting from a state of growth to one that supports reproductive activities, particularly vitellogenin (Vg) synthesis. Extensive studies in holometabolous insects have explored the degradation of the larval fat body through programmed cell death mechanisms, such as apoptosis and autophagy [4–7]. During the previtellogenic stage, the adult fat body rapidly grows through cell proliferation, preparing for large-scale Vg production during the vitellogenic phase. However, the molecular mechanisms underlying this cell proliferation and the subsequent transition of fat body cell fate from a proliferative state to one that focused on reproductive roles, especially in hemimetabolous insects, remain poorly understood.

The development and growth of insect tissues are orchestrated by a complex network of signaling pathways that regulate cell proliferation, differentiation, and tissue remodeling [8]. Key pathways, including the extracellular signal-regulated kinase/mitogen-activated protein kinase (ERK/MAPK), PI3K/TOR, Wingless/Wnt, Notch, bone morphogenetic protein (BMP), and Janus kinase-signal transducer and activator of transcription (JAK/STAT), play critical roles in these processes in insect models, such as the fruit fly, cockroach, and cricket [9–13]. These signaling cascades not only drive cellular growth but also balance somatic development with reproductive maturation. For instance, Notch signaling modulates the transition from cell proliferation to differentiation in follicle cells, ensuring the proper progression of reproductive development [14]. Exploring how these signaling pathways regulate cell proliferation offers valuable insights into the broader mechanisms that govern tissue growth and developmental transitions in insects.

Juvenile hormone (JH), a sesquiterpenoid secreted by the corpora allata, plays a vital role in stimulating vitellogenesis and egg maturation across various insect species [15–17]. JH exerts its effects through both genomic and non-genomic pathways: it binds to methoprene-tolerant (Met) and Taiman (Tai) receptor complex to mediate previtellogenic and vitellogenic effects [18–22], and rapidly activates membrane signaling cascades independently of transcription [23–27]. JH has been implicated in regulating cell proliferation and organismal growth. JH and its mimics inhibit cell proliferation in a lepidopteran imaginal disc cell line [28], while also reducing mitotic activity and preventing apoptosis in worker bee ovaries, promoting queen-like ovarian development and caste differentiation [29]. In addition, JH interacts with various signaling pathways, such as ERK/MAPK pathway, to regulate gene expression and coordinate growth, reproduction, and adaptive responses to environmental challenges in *Plutella xylostella* and *Bemisia tabaci* [30, 31]. JH also works through insulin signaling to control cell division and body size as well as further vitellogenesis of *Drosophila melanogaster* and *Pogonomyrmex rugosus* [32, 33]. Moreover, JH downregulates the miR-2/13/71 cluster, which alleviates their suppression of Notch signaling, thereby promoting the activation of Notch for JH-dependent vitellogenesis and oogenesis [34]. Despite advances in understanding the role of JH, its precise interactions with other pathways in the dynamic regulation of cell proliferation and cell fate transition remain underexplored.

In this study, using the migratory locust *Locusta migratoria* as a model, we investigated the mechanisms of fat body cell proliferation during the previtellogenic stage and the regulation in terminating this phase to facilitate the transition to Vg synthesis in the vitellogenic fat body. Our findings revealed that BMP signaling promotes fat body cell proliferation by activating key mitotic genes, such as *cyclin B* (*CycB*) and *polo-like kinase 1* (*Plk1*). Additionally, we demonstrated that JH attenuates BMP signaling during the vitellogenic phase by promoting Fzr-mediated ubiquitination and degradation of BMP signaling component, Medea. This regulatory interaction facilitates the transition from cell proliferation to Vg synthesis, effectively shifting the fat body from a growth phase to a reproductive phase. These insights underscore the critical role of BMP and JH signaling in modulating fat body cell fate and supporting reproductive functions in insects.

Results

Fat body undergoes cell fate transition during the first gonadotrophic cycle

The first gonadotrophic cycle of adult female locusts was approximately 8 days post adult eclosion (PAE). The ovaries and ovarioles remained small and white during the first 3 days, started growing and partially yellowish on day 4, and thereafter became big and yellow (Fig. 1A). *L. migratoria* possesses two *Vg* genes, *VgA* and *VgB* that are expressed in similar patterns [21]. *VgA* was selected as a representative to illustrate the developmental dynamics of *Vg* expression. As shown in Fig. 1B, the expression levels of *VgA* (GenBank: KF171066) were extremely low in the first 3 days, elevated on day 4, remarkably increased thereafter, and reached a peak at 7 days PAE. The observations indicate that the adult females underwent previtellogenic development in the first 3 days, and the vitellogenic stage started from about 4 days PAE. Detection of fat body cell proliferation by phosphorylated histone H3 (pH3) staining followed by confocal microscopy demonstrated that the number of pH3-positive cells gradually elevated in the previtellogenic period, rose to the maximum on day 4, and then remarkably decreased in the vitellogenic stage (Fig. 1C–D). Western blot confirmed

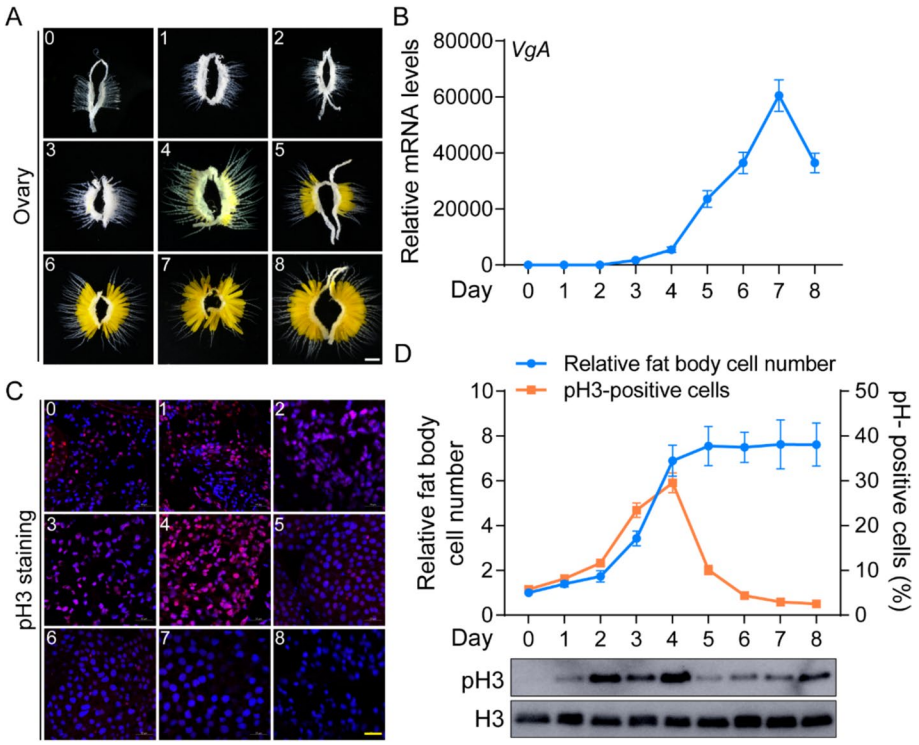

Fig. 1 Cell proliferation in the previtellogenic stage. **A** Morphology of ovaries in the adult females from day 0 to 8 of the first gonadotrophic cycle. Scale bar: 5 mm. **B** Developmental profiles of *VgA* mRNA in the fat body of adult females from day 0 to 8. $n = 8$. **C** Change of phosphor-histone H3 (pH3) staining in the fat body of adult females from day 0 to 8. pH3 staining (red) was detected using an anti-pH3 antibody to label mitotic cells. Nuclei (blue) were stained with Hoechst 33342. Scale bar: 50 μm. **D** Quantification of cell number and proportion of pH3-positive cells (upper panel), and developmental dynamics of pH3 (lower panel) in the fat body of adult females from day 0 to 8 (lower panel). Non-phosphorylated histone H3 was used as the loading control. $n = 4$

the more abundant pH3 in the previtellogenic period compared to the vitellogenic phase (Fig. 1D). Notably, the fat body cell number markedly increased in the previtellogenic period, reached to the peak on day 4, and then maintained constantly in the vitellogenic phase (Fig. 1D). Collectively, the data demonstrated that fat body underwent cell proliferation in the previtellogenic stage but ceased cell proliferation in vitellogenic phase, suggesting a switch of fat body cell fate between the previtellogenic development and vitellogenesis.

To explore the molecular basis of fat body cell fate transition, we conducted transcriptomic analysis of fat bodies collected from adult females at 0, 3, and 5 days PAE. By using the cutoff criteria of fold change > 2 and $P < 0.05$, we identified 1573 upregulated and 1494 downregulated genes at 3 days PAE (A3) compared to the day of adult ecdysis (A0), and 416 upregulated and 417 downregulated genes at 5 days PAE (A5) compared to A3 (Fig. 2A). Search for the overlap of upregulated genes at A3 but downregulated genes at A5 yielded 138 genes (Fig. 2B). Gene ontology (GO) analysis revealed the enrichment of biological processes related to cell proliferation including cell cycle, nuclear division, and DNA replication (Fig. 2C).

BMP signaling plays a pivotal role in fat body cell proliferation

We next examined six canonical signaling cascades associated with cell proliferation and tissue growth, including the ERK/MAPK, PI3K/AKT, Wingless/Wnt, Notch, BMP, and JAK/STAT signaling pathways. RNA-seq analysis of genes involved in these pathways showed that the expression levels of *decapentaplegic* (*Dpp*) and *insulin receptor 2* (*InR2*) increased at highest levels (3.45-fold and 3.21-fold, respectively) in the fat body of A3 compared to A0 (Fig. 3A), suggesting an important role of BMP signaling and PI3K/AKT pathways in fat body cell proliferation. We therefore focused this study on BMP signaling pathway. qRT-PCR showed that *Dpp* (GenBank: PQ367898) expression was significantly elevated in the previtellogenic stage (day 1–3) and early vitellogenic phase (day 4–6), but declined at late vitellogenic phase (Additional file 1: Fig. S1). The expression of *Mad* (GenBank: PQ367899) and *Medea*

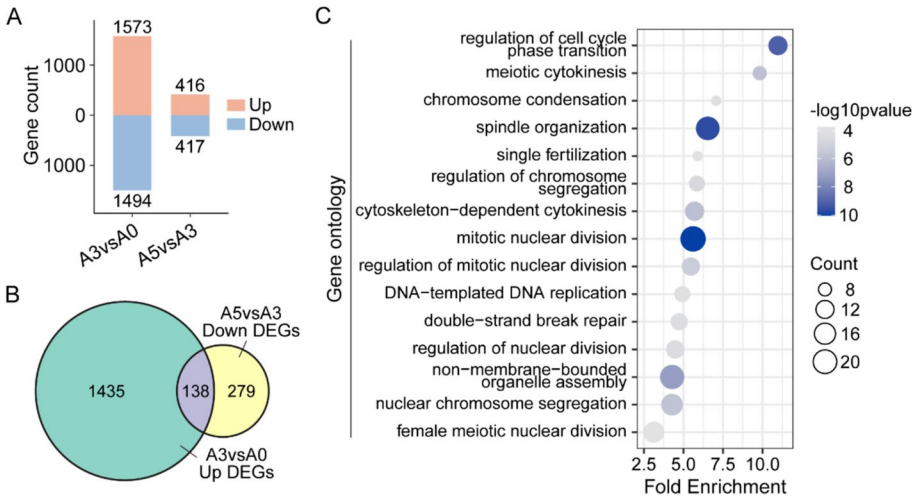

Fig. 2 RNA-seq analysis of cell fate switch from previtellogenic development to vitellogenesis. **A** The number of upregulated and downregulated genes in A3 *vs.* A0 and A5 *vs.* A3. **B** Venn diagram of A3 upregulated DEGs (*vs.* A0) and A5 downregulated DEGs (*vs.* A3) in the fat body. **C** GO enrichment analysis of 138 genes showing upregulation of biological processes in the previtellogenic phase and downregulation in the vitellogenic stage

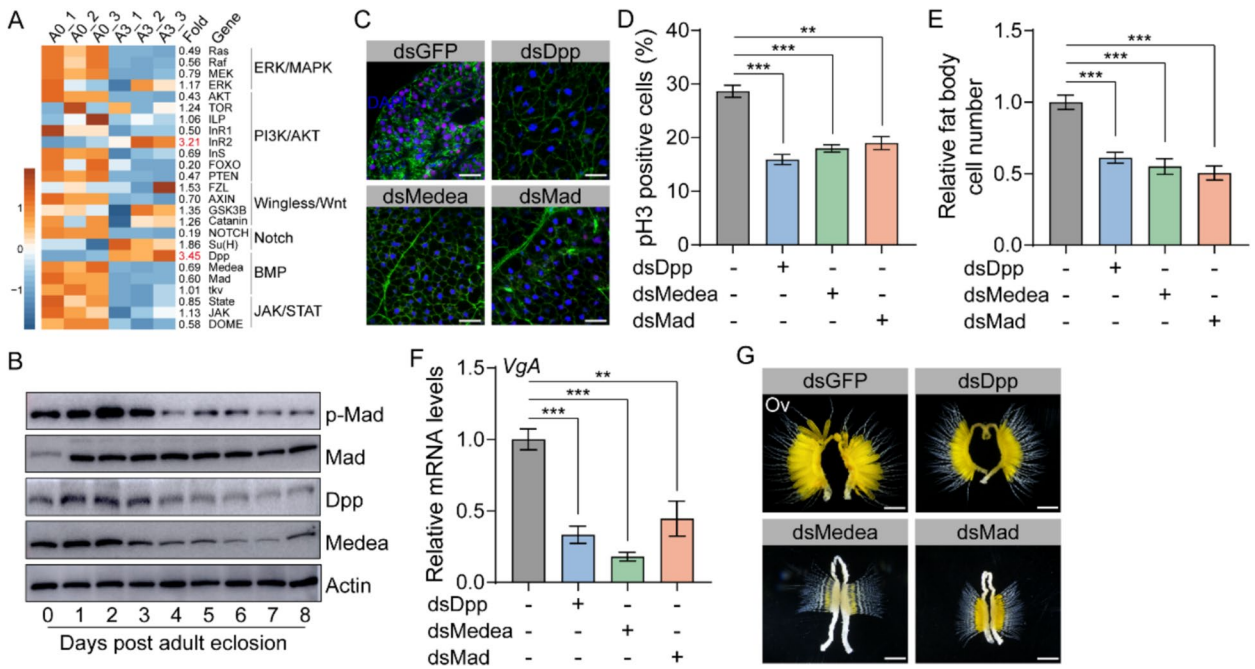

Fig. 3 Involvement of BMP signaling in cell proliferation and Vg synthesis. **A** Heatmap of genes in canonical pathways involved in cell proliferation and tissue growth. **B** Relative abundance of Dpp, Mad, phosphorylated Mad (p-Mad), and Medea in the fat body of adult females from day 0 to 8. Actin was used as the loading control. **C** pH3 staining of fat body cells subjected to *Dpp*, *Medea*, and *Mad* knockdown on day 3. pH3 (red) marks mitotic cells, Hoechst 33342 (blue) marks nuclei, and F-actin (green) was stained with Alexa Fluor 488-phalloidin. Scale bar: 50 μm. **D** Proportion of pH3-positive cells in the fat body subjected to *Dpp*, *Medea*, and *Mad* knockdown on day 3. **, $P < 0.01$ and ***, $P < 0.001$ compared with dsGFP controls. $n = 4$. **E** Statistics of fat body cell number subjected to *Dpp*, *Medea*, and *Mad* knockdown on day 6. ***, $P < 0.001$ compared with dsGFP controls. $n = 4$. **F** Relative mRNA levels of *VgA* in the fat body subjected to *Dpp*, *Medea*, and *Mad* knockdown on day 6. **, $P < 0.01$ and ***, $P < 0.001$ compared with dsGFP controls. $n = 8$. **G** Representative phenotypes of ovaries subjected to *Dpp*, *Medea*, and *Mad* knockdown on day 6. Scale bar: 5 mm

(GenBank: PQ367900) was high on day 1 and deceased thereafter, but rose to a second peak on day 6 (Additional file 1: Fig. S1). Western blot demonstrated that the abundance of Dpp, phosphorylated Mad (p-Mad), and Medea increased during the previtellogenic stage and subsequently declined in the vitellogenic phase (Fig. 3B). In the case of Mad, its abundance was low within the 12 h post adult emergence (0 day PAE), elevated on day 1, and then maintained at relatively steady levels (Fig. 3B). The data suggested the involvement of Dpp, p-Mad, and Medea in fat body cell proliferation of previtellogenic adults. In RNAi experiments, knocking down *Dpp*, *Mad*, and *Medea* reduced their transcript abundance by 83.8%, 64.7%, and 47.6%, respectively (Additional file 1: Fig. S2). Depletion of *Dpp*, *Mad*, and *Medea* led to significantly reduced pH3-positive cells (Fig. 3C). Quantitative analysis displayed that *Dpp*-, *Mad*-, and *Medea*-depleted fat bodies had 15.9%, 18.0%, and 19.0% pH3-positive cells, while 28.7% of pH3-positive cells were observed in the dsGFP control (Fig. 3D). Total cell number reduced by 40–50% in the fat bodies subjected to *Dpp*, *Mad*, and *Medea* RNAi compared to the dsGFP control (Fig. 3E). Moreover, the expression of *VgA* in the fat body as well as ovarian and oocyte growth were blocked in adults subjected to *Dpp*, *Mad*, and *Medea* RNAi (Fig. 3F and G). These data suggest that BMP signaling is essential for fat body cell proliferation. Given the potential link between BMP signaling and JH biosynthesis [35], we further examined whether *Dpp*, *Mad*, and *Medea* knockdown affects JH production in locusts. We assessed the expression levels of *Jhamt* and *Kr-h1*, two key components of JH biosynthesis and signaling pathway, but found no significant changes in their expression upon BMP signaling knockdown (Additional file 1: Fig. S3). Taken together, our data demonstrate that BMP signaling is crucial for fat body cell proliferation during the previtellogenic development, independently of its role in JH biosynthesis.

Mad/Medea stimulates *CycB* and *Plk1* transcription for cell proliferation

Following RNA-seq-based gene profiling, we selected 17 genes out of 138 that are involved in cell proliferation and mitotic cell cycle progression for further study. qRT-PCR was conducted to assess the effect of *Dpp*, *Mad*, and *Medea* RNAi on the expression of these genes over 3 days, when fat body cell proliferation is robust. Among the downregulated genes, we identified Myb, a transcription factor, known to be crucial for cell proliferation and mitosis. Additionally, genes associated with the kinetochore-associated NDC80 complex (Ndc80) responsible for chromosome segregation, cyclin A (CycA) and CycB involved in the G2/M phase transition, serine/threonine-protein kinase (Plk1) essential for centrosome maturation and spindle assembly, and cell division cycle protein 20 (Cdc20), which regulates the ubiquitin ligase activity of the anaphase-promoting complex/cyclosome (APC/C), were also downregulated following knockdown of *Dpp*, *Mad*, and *Medea* (Fig. 4A).

Analysis of the 3 kb upstream sequences of the six downregulated genes revealed a conserved BMP response element (BRE, GGCGCC) within the promoter regions of *CycB* (nt −1720 to −1715, GenBank: PQ367901) and *Plk1* (nt −2067 to −2061, GenBank: PQ367902) (Additional file 1: Fig. S4). This element is recognized as a binding site for the Mad/Medea complex, which is involved in transcriptional regulation in both mouse and *Drosophila* [36, 37]. To determine whether BMP signaling regulates *CycB* and *Plk1* transcription in locusts, we expressed locust Mad and Medea in S2 cells and performed luciferase reporter assays and electrophoretic mobility shift assay (EMSA). For the luciferase reporter assays, we cloned the segments of 4×

(See figure on next page.)

Fig. 4 Regulation of BMP signaling molecules in mitotic gene transcription. **A** Heatmap of genes related to cell cycle transition in the fat body of dsDpp-, dsMedea-, and dsMad-injected adult females on day 3. *, $P < 0.05$ compared with dsGFP controls. $n = 4$. **B** Left panel: Luciferase reporter assays using *Drosophila* S2 cells transfected with pGL4.10/*CycB* + pAc5.1/V5 empty vector, pGL4.10/*CycB* + pAc5.1/V5-Mad, pGL4.10/*CycB* + pAc5.1/V5-Medea, and pGL4.10/*CycB* + pAc5.1/V5-Mad + pAc5.1/V5-Medea. Right panel: Luciferase reporter assays using S2 cells transfected with pGL4.10/*Plk1* + pAc5.1/V5 empty vector, pGL4.10/*Plk1* + pAc5.1/V5-Mad, pGL4.10/*Plk1* + pAc5.1/V5-Medea, and pGL4.10/*Plk1* + pAc5.1/V5-Mad + pAc5.1/V5-Medea. ***, $P < 0.001$ compared with control. $n = 4$. **C** EMSA using the biotin-labeled *CycB* (left), biotin-labeled *Plk1* (right), and non-labeled cold probe incubated with nuclear protein extracts from *Drosophila* S2 cells with expressed V5-Mad and V5-Medea. α-V5, anti-V5 antibody; α-IgG, a nonspecific antibody. The arrows indicate the specific bands. **D** Upper panel: pH3 staining of fat body cells in dsCycB- and dsPlk1-treated adult females on day 3. pH3 (red) marks mitotic cells, Hoechst 33342 (blue) marks nuclei, and phalloidin (green) marks F-actin. Scale bar: 50 μm. Lower panel: representative phenotypes of ovaries in dsCycB- and dsPlk1-treated adult females on day 6. Scale bar: 5 mm. **E** Proportion of pH3-positive cells in the fat body of dsCycB- and dsPlk1-treated adult females on day 3. ***, $P < 0.001$ compared with dsGFP. $n = 4$. **F** Statistics of fat body cell number in the fat body of dsCycB- and dsPlk1-treated adult females on day 6. ***, $P < 0.001$ compared with dsGFP. $n = 4$. **G** Relative mRNA levels of *VgA* in the fat body of dsCycB- and dsPlk1-treated adult females on day 6. *, $P < 0.05$ and **, $P < 0.01$ compared with dsGFP. $n = 8$

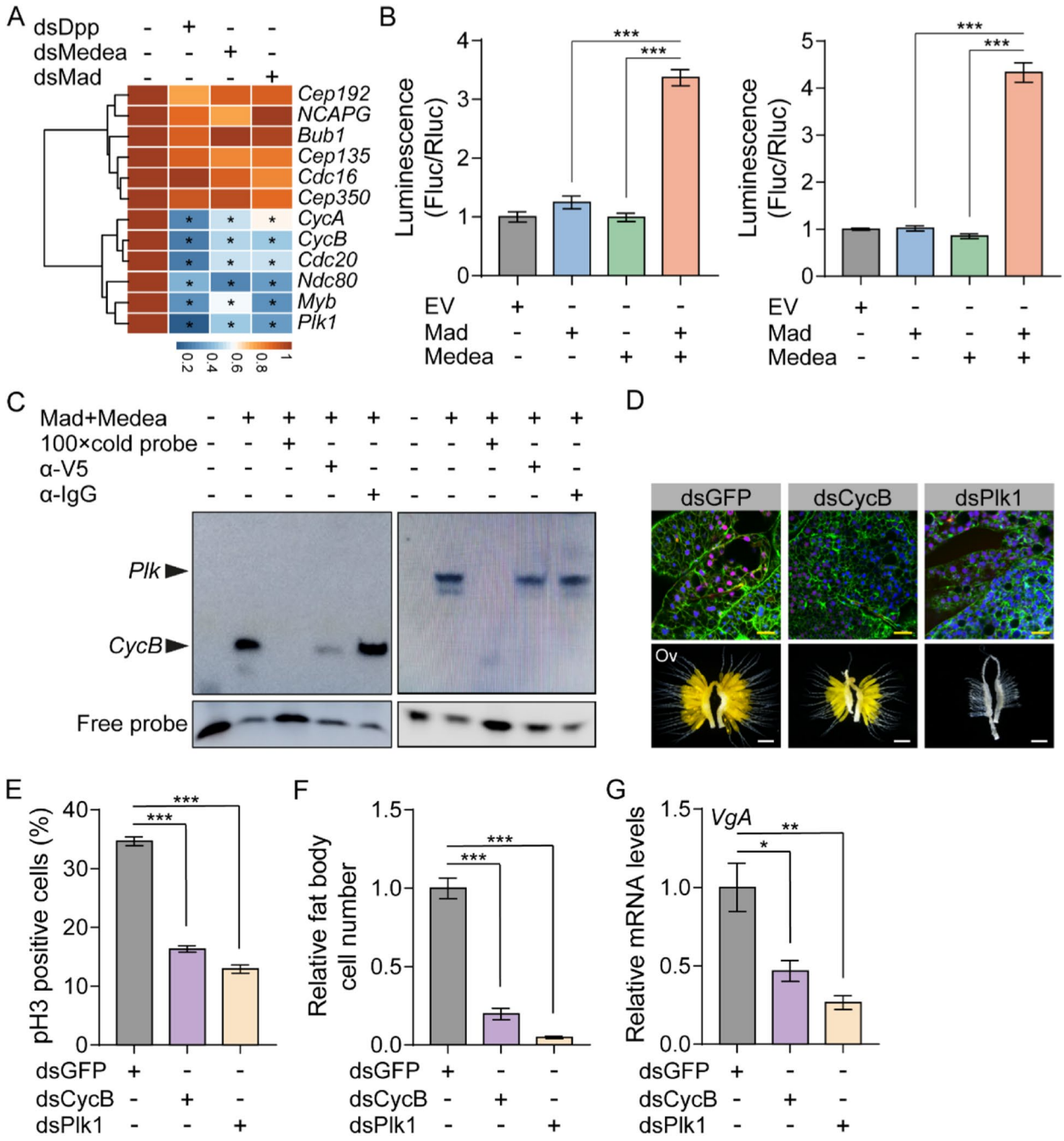

Fig. 4 (See legend on previous page.)

$CycB^{-1728\ to-1707}$ and $4\times$ $Plk1^{-2074\ to-2053}$, containing the BRE motifs, into the pGL4.10 vector. Co-transfection with pAc5.1/V5-Mad and pAc5.1/V5-Medea resulted in a more than 3-fold increase in *CycB* and *Plk1* reporter activities compared to the pAc5.1/V5 empty control (Fig. 4B). In contrast, co-transfection with either pAc5.1/V5-Mad or pAc5.1/V5-Medea alone did not significantly induce *CycB* or *Plk1* reporter activity (Fig. 4B). To further characterize the binding of the Mad/Medea complex to the BRE in the *CycB* and *Plk1* promoters, we performed EMSA using nuclear extracts from S2 cells co-transfected with pAc5.1/V5-Mad and pAc5.1/V5-Medea. We utilized 22-mer nucleotide probes corresponding to the BRE-containing sequences in the *CycB* and *Plk1* promoters (Additional file 1: Fig. S4). Specific bands were detected with biotin-labeled *CycB* and *Plk1* probes (lane 2), and

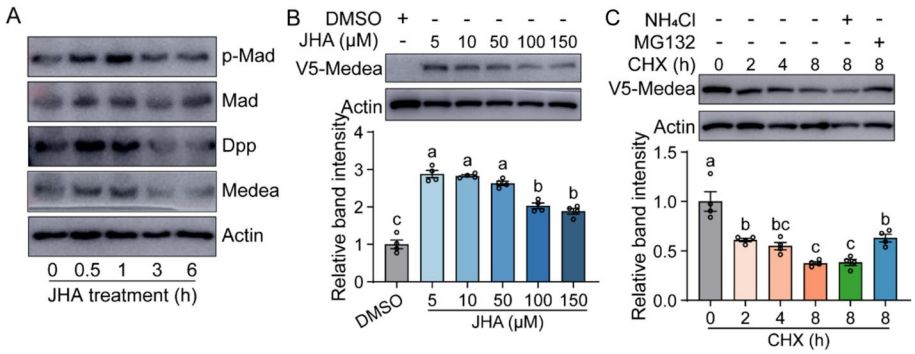

Fig. 5 Medea proteolysis in the vitellogenic fat body. **A** Relative abundance of Dpp, Mad, p-Mad, and Medea in the fat body of JH-deprived adult females further treated with JH analog, methoprene (JHA) for 0.5, 1, 3, and 6 h. **B** Upper panel: immunoblots showing the effect of JHA on the stability of expressed V5-Medea in *Drosophila* S2 cells. The cells were treated with JHA at a dose of 5, 10, 50, 100, and 150 μM. Lower panel: quantification of the relative band intensity. $n = 4$. **C** Upper panel: immunoblots showing the effect of lysosome or proteasome inhibitors on Medea stability. The cells were pre-treated with methoprene and added with CHX for indicated intervals and corresponding inhibitors NH_4Cl (for lysosome) and MG132 (for proteasome). Lower panel: quantification of the relative band intensity. Means labeled with different letters indicate significant difference at $P < 0.05$. $n = 4$

these bands were abolished with a 100 ×molar excess of unlabeled *CycB* and *Plk1* probes (lane 3). Pre-incubation with an anti-V5 antibody (lane 4) eliminated or reduced the specific bands, while pre-incubation with IgG (lane 5) had no effect on their mobility or intensity (Fig. 4C). These findings confirmed that the Mad/Medea complex binds to the *CycB* and *Plk1* promoters and stimulates their transcription.

To further assess the roles of CycB and Plk1 in cell proliferation in the previtellogenic stage, we conducted RNAi experiments targeting *CycB* and *Plk1*. Knockdown of *CycB* led to an 88.3% reduction in its mRNA levels in the fat body of adult females, while *Plk1* RNAi resulted in a 94.8% reduction in *Plk1* mRNA levels (Additional file 1: Fig. S5). As expected, both *CycB*- and *Plk1*-depleted fat bodies exhibited significantly fewer pH3-positive cells and lower total cell counts compared to the dsGFP control (Fig. 4D–F). Consequently, *VgA* mRNA levels were notably reduced in the fat bodies of *CycB*- and *Plk1*-depleted adult females (Fig. 4G), which was associated with severely arrested ovarian growth (Fig. 4D). These observations underscored the pivotal role of the BMP signaling-CycB/Plk1 cascade in regulating cell proliferation and previtellogenic growth.

High levels of JH cause Medea degradation

During the vitellogenic phase, fat body cells cease proliferation (Fig. 1C–D) and undergo a cell fate transition to support extensive Vg synthesis [21, 38–40], making the suppression of BMP signaling crucial. A previous study reported a sharp increase in JH titers around day 4 during the early vitellogenic phase [41]. Initially, we applied methoprene, a JH analog (JHA), topically to newly emerged adults with low JH titers and monitored cell proliferation at day 2 and day 4 post-treatment. JHA treatment led to a significant reduction in the percentage of pH3-positive cells and the relative fat body cell number at both time points (Additional file 1: Fig. S6). These phenotypes closely resemble those observed upon knockdown of BMP signaling components, supporting the hypothesis that higher JH levels may inhibit cell proliferation by repressing BMP signaling. The results presented in Fig. 3B showed a decline in the abundance of Dpp, p-Mad, and Medea in the vitellogenic fat bodies, suggesting the responsiveness of BMP signaling to JH. To further confirm this, we performed western blot analyses using protein extracts from the fat bodies of JH-deprived adult females at 6 days PAE, and those further treated with JHA for 0.5 to 6 h. As a result, Dpp, p-Mad, and Medea were more abundant after shorter JH exposure, while prolonged exposure led to a marked inhibition of BMP signaling (Fig. 5A). The results indicated that the elevated JH titers during the vitellogenic phase attenuate the effect of BMP signaling on fat body cell proliferation, shifting the cell fate towards Vg synthesis.

Given that Medea degradation is a key factor in the termination of BMP signaling [42], and considering the observed decrease in Medea protein levels at 4–8 days PAE (Fig. 3B), we focused on exploring the regulatory role of JH in Medea protein stability. When methoprene was added to S2 cells expressing V5-Medea at doses ranging from 5 to 150 μM, Medea became unstable at higher methoprene doses (Fig. 5B). Cycloheximide (CHX), a global translational inhibitor, is commonly used to study the degradation of short-lived proteins. We conducted pulse-chase experiments in S2 cells expressing

V5-Medea, treated with methoprene followed by addition of CHX for 2, 4, and 8 h. Western blot analyses confirmed that Medea is a short-lived protein (Fig. 5C). Moreover, we demonstrated that Medea undergoes proteosome-mediated protein degradation, as indicated by the effective inhibition of Medea degradation after treatment with the proteosome inhibitor MG132 (Fig. 5C). Therefore, Medea protein is likely subjected to JH-induced proteolysis in the vitellogenic fat body, contributing to the attenuation of BMP signaling and thus cell fate shift.

Medea is ubiquitinated by Fzr

To elucidate the mechanisms underlying Medea degradation, we analyzed the 416 genes upregulated at A5 compared to A3. A Kyoto Encyclopedia of Genes and Genomes (KEGG) enrichment analysis revealed that ubiquitin-mediated proteolysis was significantly activated during the vitellogenic phase (Additional file 1: Fig. S7). The APC/C is an E3 ubiquitin ligase that targets specific proteins, such as mitotic cyclins, for degradation by the 26S proteosome, thereby facilitating cell cycle progression [43]. Since the activity of APC/C depends on the scaffold protein fizzy-related protein (Fzr), homologous to mammalian Cdh1 [44], we investigated the role of Fzr (GenBank: PQ367903) in Medea proteolysis in locusts. Indeed, co-transfection of Flag-Fzr and V5-Medea in S2 cells accelerated Medea degradation (Fig. 6A), suggesting the involvement of Fzr in Medea proteolysis.

Proteins targeted by the APC/C complex often contain destruction boxes (D box), characterized by a consensus sequence RXXLXXXXD/E/N [45]. Sequence alignment revealed a conserved D box (amino acids 473–481) in the locust Medea protein, which has been documented as crucial for Fzr-mediated protein degradation in mammals [46–51] (Additional file 1: Fig. S8). To investigate the role of the D box in involving Fzr-mediated Medea degradation, we co-transfected D box-depleted V5-Medea ($Medea^{\Delta D-box}$) with Flag-Fzr in methoprene-pretreated S2 cells, followed by the addition of CHX at intervals. The results showed that Fzr had no obvious effect on the degradation of D box-depleted V5-Medea (Fig. 6B). Computational prediction using BDM-PUB (V1.0) software identified the lysine residue at position 49 (Lys^{49}) as a potential ubiquitination site with the highest likelihood. To validate the role of Fzr in targeting Lys^{49} of Medea, we constructed a mutated V5-Medea ($Medea^{K49E}$, Lys^{49} to Glu^{49}) and co-transfected it with Flag-Fzr into S2 cells treated with methoprene and CHX. As shown in Fig. 6C, the degradation of V5-$Medea^{K49E}$ was slower compared to the wild-type V5-Medea ($Medea^{WT}$) (Fig. 6C). To further determine whether Fzr promotes the ubiquitination of Medea, we conducted a cell-based ubiquitination assay in S2 cells. The smeared bands of ubiquitinated Medea were detected in the nucleoprotein fractions when was co-transfected with Flag-Fzr, indicating that Fzr enhances Medea poly-ubiquitination (Fig. 6D). These data together suggested that upon entering the vitellogenic phase, Medea protein undergoes Fzr-executed ubiquitination and induces cell fate transition.

Discussion

BMP signaling and cell proliferation

In this study, one of the primary findings is the upregulation of BMP pathway components during the previtellogenic stage, which corresponds with increased mitotic activity. Knockdown of the components led to a significant reduction in cell proliferation, highlighting the importance of BMP signaling in ensuring that the fat body grows to a sufficient size to support reproductive demands. In the American cockroach *Periplaneta americana*, BMP signaling is crucial for promoting blastema cell proliferation during leg regeneration [52]. In *Drosophila*, BMP signaling establishes a phosphorylated Mad gradient to ensure asymmetric stem cell division and balanced differentiation [53]. Additionally, in the *Drosophila* intestine, BMP signaling precisely regulates cell proliferation during tissue regeneration by modulating receptor activation and internalization [54]. During wing development, BMP coordinates cell proliferation and tissue patterning by aligning signal distribution with the changing 3D tissue structure [55]. In addition to promoting cell proliferation, BMP signaling has been implicated in lipid metabolism by maintaining lipid homeostasis through the regulation of lipolysis [56]. This ensures that energy reserves are presented and mobilized at appropriate stages to meet the metabolic demands of development and reproduction. These findings are consistent with the broader role of BMP in regulating cell division, lipid homeostasis, and tissue growth across different species. In the future, we aim to uncover the molecular mechanisms by which developmental initiation signals activate BMP pathway to trigger cell proliferation and fat body growth during the previtellogenic stage.

JH and Fzr-mediated Medea ubiquitination

Our study demonstrated that the elevated JH titers during the vitellogenic phase diminish BMP activity through Fzr-mediated ubiquitination and degradation of Medea, thereby halting cell proliferation and initiating Vg synthesis. This highlights the dynamic interaction between JH and BMP signals. In the cricket *Gryllus bimaculatus*, TGF-β/BMP signaling delicately controls insect metamorphosis by regulating JH production, facilitating the transition from nymph to adult [57]. Beyond JH-induced antagonization, BMP signaling can also be attenuated by

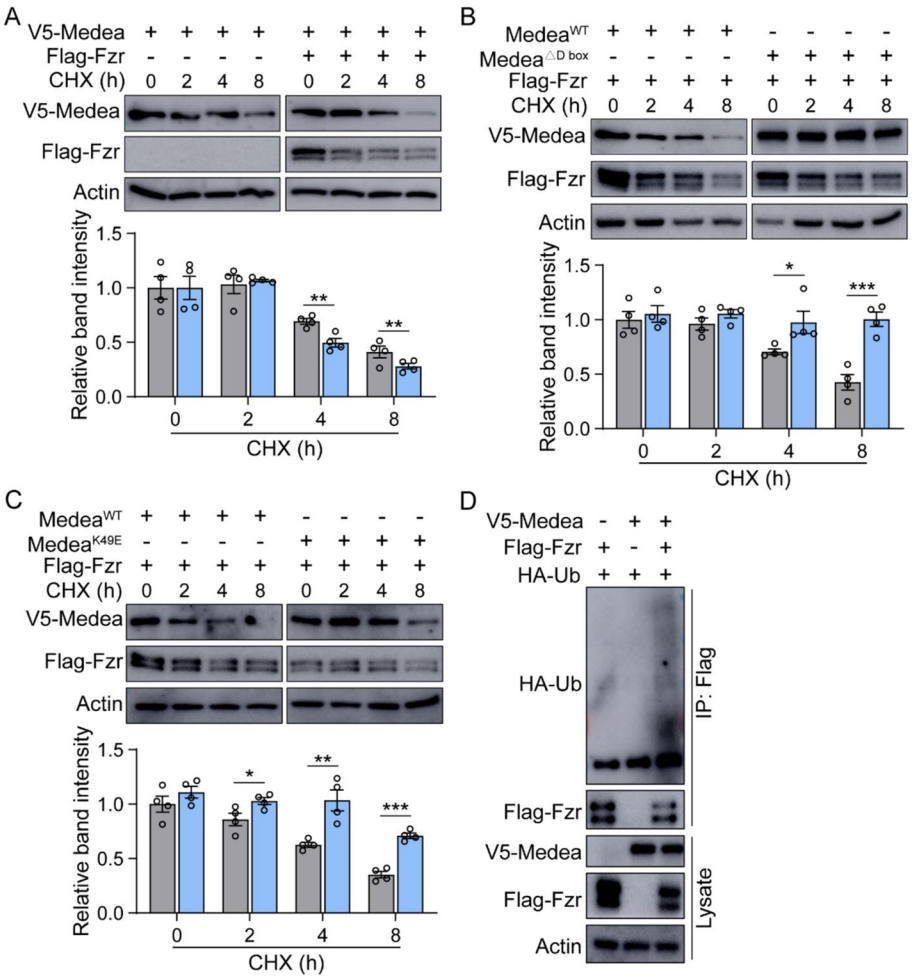

Fig. 6 Ubiquitination and destabilization of Medea by Fzr. **A** Upper panel: immunoblots showing the effect of Fzr on Medea protein degradation. Lower panel: quantification of the relative band intensity. Blue bar: band intensity of samples co-expressing V5-Medea and Flag-Fzr. Gray bar: band intensity of samples expressing V5-Medea alone (control). **, $P < 0.01$ compared with control. $n = 4$. **B** Upper panel: immunoblots showing the effects of D box mutation on Medea degradation. Lower panel: quantification of the relative band intensity. Blue bar: band intensity of samples co-expressing D box-depleted Medea ($Medea^{\Delta D-box}$) and Flag-Fzr. Gray bar: band intensity of samples co-expressing intact Medea ($Medea^{WT}$) and Flag-Fzr. *, $P < 0.05$ and **, $P < 0.01$ compared with control. $n = 4$. **C** Upper panel: immunoblots showing the effects of Lys^{49} site mutation on Medea degradation. Lower panel: quantification of the relative band intensity. Blue bar: band intensity of samples co-expressing Lys^{49} mutated Medea ($Medea^{K49E}$) and Flag-Fzr. Gray bar: band intensity of samples co-expressing wild-type Medea ($Medea^{WT}$) and Flag-Fzr. *, $P < 0.05$, **, $P < 0.01$, and ***, $P < 0.001$ compared with control. $n = 4$. **D** In vitro ubiquitination assays showing the direct effect of Fzr on Medea degradation. Proteins were immunoprecipitated using anti-Flag antibody and probed for ubiquitinated Medea using anti-HA antibody

other pathways such as MAPK-mediated phosphorylation of Smad1/5/8, which promotes their ubiquitination and degradation, and PI3 K/Akt pathway interference with Smad3/4 activity, leading to the cessation of BMP signal transduction [58, 59]. In our study, JH acts as a molecular switch that shifts cell fate and repurposes the fat body from a proliferative state to one focused on Vg synthesis. In fact, the dual role of fat body in tissue growth and reproduction is not unique to *L. migratoria*. In the holometabolous insect like *Aedes aegypti*, fat body reconstruction begins after pupation, with Vg production triggered after a blood meal in adulthood [15, 60]. In contrast, the hemimetabolous insects like locusts must continuously balance fat body growth and vitellogenesis throughout adulthood, as they lack the distinct larval-to-adult transition seen in holometabolous species. In addition, we identified Fzr as a key regulator in this process. Fzr promotes Medea ubiquitination and degradation, leading to the downregulation of mitotic genes and facilitating the switch from cell proliferation to polyploidization, which is essential for large-scale Vg production [21, 38–40]. This regulatory mechanism is consistent with

findings in other species, such as *Drosophila* and *Bombyx mori*, where Fzr promotes cell cycle switch from mitotic cycle to endocycle in various tissues [61–65]. Taken together, the ability of JH to regulate both transcriptional and post-translational processes allow rapid responses to hormonal cues, highlighting its dual genomic and non-genomic actions across different insect orders. However, the gap between JH and Fzr remains underexplored. Future research could focus on elucidating the regulatory mechanisms, which may provide deeper insights into how JH modulates BMP signaling and fat body cell fate.

Conclusions

In summary, this study uncovers the critical role of BMP signaling in regulating fat body cell proliferation and demonstrates how JH modulates this pathway to coordinate the transition from growth to Vg synthesis (Fig. 7). The identification of Fzr-mediated Medea degradation as a key mechanism by which JH antagonizes BMP signaling and changes fat body cell fate during the vitellogenic phase deepens our understanding of hormone-driven insect reproduction. These findings not only advance our knowledge of insect reproductive physiology but also offer potential targets for pest control through the disruption of hormonal and signaling pathways.

Methods

Insect rearing

The gregarious phase of *L. migratoria* was maintained under standard conditions as described previously[21]. JH-deprived adult females were obtained by application of precocene III (Sigma-Aldrich) at a dose of 500 μg per locust within 6 h PAE. These locusts were maintained for 6 days after precocene treatment to ensure effective JH deprivation. At day 6, *s*-(+)-methoprene (Santa Cruz Biotech) was applied at a dose of 150 μg per locust. Locusts were dissected at different time points after methoprene application, specifically 0.5, 1, 3, or 6 h post-treatment. The newly emerged female adults were applied for 150 μg methoprene for 2 and 4 days.

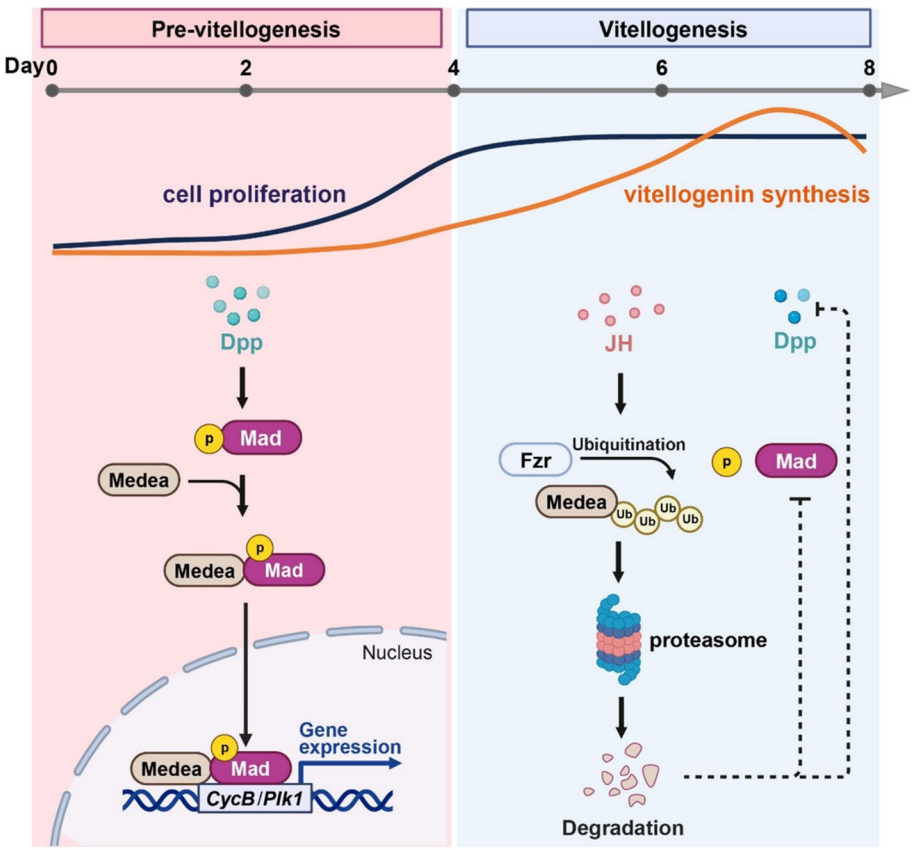

Fig. 7 Interplay of JH and BMP signaling in the regulation of fat body cell fate. During the previtellogenic stage, activated BMP signaling stimulates the expression of *CycB* and *Plk1*, promoting cell proliferation and facilitating fat body remodeling. In the vitellogenic fat body, high levels of JH induce the Fzr-mediated ubiquitination and degradation of Medea, attenuating the BMP pathway. Inhibitory BMP pathway halts mitosis and shifts the cell fate towards Vg synthesis. Solid lines and arrow heads indicate positive regulation. Dotted lines and T-bars represent negative effect

RNA sequencing and data processing

Total RNA was extracted from fat bodies of adult locusts at 12 h, 3, and 5 days PAE (three biological replicates, each consisting of four individuals) using TRIzol reagent (Invitrogen). cDNA libraries were constructed according to Illumina's protocols. Raw sequencing data were filtered and corrected for quality. The resulting reads were then mapped to locust genome sequence using HISAT2. Differentially expressed genes (DEGs) with statistical significance ($P < 0.05$) were identified and enriched in each comparison.

Eukaryotic cell culture and protein expression

Protein coding sequences of Mad (nt 1–1368), Medea (nt 1–2229), Fzr (nt 1–1530), and Ub (nt 1–696) were individually cloned into pAc5.1/V5 or pAc5.1/Flag vectors (Invitrogen). Site-directed mutagenesis was performed to generate Medea$^{\Delta D-box}$ (D-box depletion) and Medea^{K49E} (Lys^{49} to Glu^{49} substitution) variants using Q5 Site-Directed Mutagenesis Kit (New England Biolabs). Primers used for recombinant vector construction and site-directed mutagenesis are listed in Table S1 (Additional file 1). *Drosophila* S2 cells were cultured in Schneider's *Drosophila* medium supplemented with 10% fetal bovine serum (FBS) at 28 °C. S2 cells were transfected with the recombinant vectors using Lipofectamine 3000 (Invitrogen). Methoprene was added at concentrations ranging from 5 to 150 μM for 3 h. MG132 (MedChemExpress) at 50 μM, NH_4Cl (Beyotime) at 10 mM, and cycloheximide (CHX, MedChemExpress) were added at 50 μM, 10 mM, and 50 μg/ml, separately, followed by methoprene at 50 μM.

qRT-PCR

First-stranded cDNA was synthesized from total RNA using the FastKing RT kit with gDNase (Tiangen). qRT-PCR were performed using a RealMasterMix SYBR Green kit (Tiangen) on a LightCycler 96 system (Roche), initiated at 95 °C for 15 min, followed by 40 cycles at 95 °C for 10 s, 58 °C for 20 s, and 72 °C for 30 s. Relative expression levels were calculated using $2^{-\Delta\Delta Ct}$ method and normalized to the expression of *β-actin*. Primers used for qRT-PCR are listed in Table S1 (Additional file 1).

Western blot and immunoprecipitation

Protein extracts from insect fat body and *Drosophila* S2 cells were isolated using ice-cold lysis buffer containing 150 mM NaCl, 50 mM Tris–HCl (pH 7.4), 1 mM EDTA, 1% Nonidet P-40, 1% Triton X-100, 0.5% sodium deoxycholate, 1 mM PMSF plus protease, and a cocktail of protease and phosphatase inhibitors (Roche). Lysates were cleared by centrifugation at 12,000 rpm for 15 min at 4 °C, then subjected to 8% sodium dodecylsulfate polyacrylamide gel electrophoresis (SDS-PAGE) and transferred to polyvinylidene fluoride (PVDF) membrane (Millipore). Western blots were conducted using primary antibodies and corresponding horseradish peroxidase (HRP)-conjugated secondary antibodies (TransGen Biotech) and visualized with Superstar ECL Plus Ready-to-use Kit (Boster). β-Actin was used as a loading control.

For immunoprecipitation, precleared lysates were incubated with anti-Flag antibody (MBL) for 60 min at 4 °C. The immunocomplexes were captured with protein-A agarose (Sigma-Aldrich) and incubated overnight at 4 °C. After washing, the complexes were eluted in Laemmli sample buffer, followed by western blots with anti-Fzr (Santa Cruz Biotech) antibodies.

For in vivo ubiquitination assay, S2 cell were co-transfected with HA-tagged Ub, Flag-tagged Fzr, and V5-tagged Medea constructs. At 48 h after transfection, cells were treated with 50 μM MG132 for 8 h, and the nuclear extracts were harvested using NE-PER Nuclear and Cytoplasmic Extraction Reagents kit (Thermo Fisher Scientific) according to the manufacturer's instructions. Following precipitation with anti-Flag antibody for 60 min at 4 °C, the precipitates were subjected to western blot using anti-HA antibody (MBL) to detect Medea ubiquitination by Fzr.

RNAi, tissue imaging, and confocal microscopy

cDNA templates were amplified by PCR, cloned into pGEM-T vector (Tiangen), and confirmed by sequencing. Double-stranded RNAs (dsRNAs) were synthesized by in vitro transcription with T7 RiboMAX Expression RNAi System (Promega). Newly emerged adult females were intra-abdominally injected with 15 μg of dsRNA and boosted on day 3. Injection of green fluorescent protein (GFP) dsRNA was used as the mock control. Primers used for RNAi are listed in Table S1 (Additional file 1).

For RNAi experiments, the assessment of *VgA* mRNA levels via qRT-PCR and ovary phenotypes were examined on day 6, and the immunostaining was performed on day 3. Ovaries were photographed by a Leica M205 C stereomicroscope. For immunostaining, the naturally developmental and dsRNA-subjected fat bodies were dissected, fixed in 4% paraformaldehyde, and permeabilized in 0.3% Triton X-100. Immunostaining was conducted using an anti-pH3 antibody (Cell Signaling Technology) and an Alexa Fluor 594-conjugated secondary antibody (Invitrogen). To determine the percentage of pH3-positive cells, more than 100 cells were randomly selected, and the experiment was repeated three times. F-actin

and nuclei were stained with 0.165 μM phalloidin-Alexa Fluor 488 (Invitrogen) and 5 μM Hoechst 33342 (Sigma-Aldrich), respectively. Cell images were captured with a ZEISS LSM 710 laser confocal microscope and processed with ZEN2012 software (Carl Zeiss).

Flow cytometry

For RNAi experiments, the statistics of cell count were conducted on day 6. In brief, the naturally developmental and 6-day-old dsRNA-subjected fat bodies were homogenized using a Dounce homogenizer. Cells were collected by centrifugation (800 ×g), fixed in 70% ethanol overnight, and incubated for 2 h at 4 °C in a solution containing 50 μg/ml propidium iodide (Sigma), 100 μg/ml RNaseA (Promega), and 0.2% Triton X-100 in PBS. The cells were filtered through 300-mesh cell strainers (BD Falcon) and analyzed using a BD FACSCalibur Flow Cytometry System with Flowjo 7.6.1 software (BD Biosciences). Cell counts were obtained from total fat body preparations, with four independent experiments conducted for each treatment. Locust brain nuclei were used as the diploid reference control.

Dual luciferase reporter assay

The promoter regions of *CycB* and *Plk1*, which bears the BMP response element (BRE, GGCGCC), specifically the segments 4× CycB$^{-1728\ to-1707}$ and 4× Plk1$^{-2074\ to-2053}$, were separately ligated into pGL4.10 vector (Promega) and verified by sequencing. S2 cells were co-transfected with pGL4.10/4 ×CycB$^{-1728\ to-1707}$ or 4× Plk1$^{-2074\ to-2053}$ constructs or pGL4.10 empty vector, along with recombinant vectors expressing pAc5.1/V5-Mad$^{1-1368}$ and pAc5.1/V5-Medea$^{1-2229}$ using Lipofectamine 3000 (Invitrogen). After 48 h, luciferase activity was then measured using a Dual-luciferase Reporter Assay System and a GloMax 96 Microplate Luminometer (Promega).

Electrophoretic mobility shift assay (EMSA)

Nuclear extracts from S2 cells were isolated using NE-PER Nuclear and Cytoplasmic Extraction Reagents kit. The *CycB* probe (5′-TTCAACATGGCGCCGCATTCTC-3′) and *Plk1* probe (5′-AATCATTTGGCGCCTGTA CATG-3′) were end-labeled with biotin and incubated with nuclear protein extracts using the LightShift Chemiluminescent EMSA kit (Thermo Fisher Scientific). For the competition assay, a 100 ×molar excess of unlabeled *CycB* or *Plk1* probe was added into the binding reaction to compete with the labeled probes. In the supershift assays, the nuclear extracts were pre-incubated with an anti-V5 antibody (MBL) or the control IgG (Sigma-Aldrich) for 1 h at 4 °C before adding the labeled probes. The resulting DNA–protein complex were separated on 5% native polyacrylamide gels and visualized using an Amersham Imager 600 (GE healthcare).

Data analysis

Statistics analyses were performed using Student's *t*-test or one-way analysis of variance (ANOVA) with Tukey's *post hoc* test, performed with SPSS 22.0 software. Significant difference was considered at $P < 0.05$. All data are presented as means ± standard error of the mean (SEM).

Abbreviations

Vg	Vitellogenin
Dpp	Decapentaplegic
CycB	Cyclin B
Plk1	Polo-like kinase 1
Fzr	Fizzy-related protein
BMP	Bone morphogenetic protein
JH	Juvenile hormone
Met	Methoprene-tolerant
Tai	Taiman
PAE	Post adult eclosion
pH3	Phosphorylated histone H3
CHX	Cycloheximide
DEG	Differentially expressed genes
GO	Gene ontology
KEGG	Kyoto Encyclopedia of Genes and Genomes

Supplementary Information

The online version contains supplementary material available at https://doi.org/10.1186/s12915-025-02247-2.

Additional file 1: Figures S1–S8. Fig. S1 qRT-PCR showing the developmental profile of BMP signaling components *Dpp*, *Medea*, and *Mad* in the fat body of adult females from day 0 to 8 post adult eclosion. Fig. S2 RNAi efficiency of *Dpp*, *Medea*, and *Mad* in the fat body of adult females on day 6. Fig. S3 Effect of BMP signaling knockdown on the expression of JH biosynthesis and signaling pathway. Fig. S4 Alignment of cDNA sequences containing BMP response elementin the promoter of *Id1*, *Id2*, and *Id3* from *Mus musculus*, *FMRFa* from *Drosophila*, and *CycB* and *Plk1* from *L. migratoria*. Fig. S5 RNAi efficiency of *CycB* and *Plk1* in the fat body of adult females on day 6. Fig. S6 Suppression of fat body cell proliferation by methoprene in newly emerged adults. Fig. S7 KEGG enrichment analysis of the genes upregulated at A5 compared to A3. Fig. S8 Alignment of DNA sequences containing destruction box. Table S1 Primers used for qRT-PCR, RNAi, and site-directed mutagenesis.

Additional file 2: Original western blot data

Authors' contributions

ZXW and STZ designed the research. ZXW and STZ wrote the manuscript. ZXW, WXZ, MYL, and QJH performed the experiments. YL1 (YYL) performed the bioinformatics analysis. YYH, YL2, SQZ, and HHS contributed to data analysis. All authors read and approved the final manuscript.

Funding

This work was supported by grants from the National Natural Science Foundation of China (32172389 and U22A20482) and Natural Science Foundation of Henan Province (232300421029). It was also partially supported by grant from the National Natural Science Foundation of China (32102215).

Data availability

The datasets supporting the conclusions of this article are included within the article and its additional files. Gene coding sequences obtained in this study have been deposited in the NCBI GenBank database under the accession numbers: Dpp: PQ367898 (https://www.ncbi.nlm.nih.gov/nuccore/PQ367898.1/) [66]; Mad PQ367899 (https://www.ncbi.nlm.nih.gov/nuccore/PQ367898.1/)

[67]; Medea: PQ367900 (https://www.ncbi.nlm.nih.gov/nuccore/PQ367900.1/) [68]; CycB: PQ367901 (https://www.ncbi.nlm.nih.gov/nuccore/PQ367901.1/) [69]; Plk1: PQ367902 (https://www.ncbi.nlm.nih.gov/nuccore/PQ367902.1/) [70] and Fzr: PQ367903 (https://www.ncbi.nlm.nih.gov/nuccore/PQ367903.1/) [71]. RNA-seq data that support the findings of this study have been deposited into Sequence Read Archive Database of the NCBI under the Bioproject PRJNA1165726 (https://www.ncbi.nlm.nih.gov/bioproject/PRJNA1165726/) [72].

Declarations

Ethics approval and consent to participate
Not applicable.

Consent for publication
Not applicable.

Competing interests
The authors declare no competing interests.

Received: 26 October 2024 Accepted: 13 May 2025
Published online: 28 May 2025

References
1. Arrese EL, Soulages JL. Insect fat body: energy, metabolism, and regulation. Annu Rev Entomol. 2010;55:207–25.
2. Li S, Yu X, Feng Q. Fat body biology in the last decade. Annu Rev Entomol. 2019;64:315–33.
3. Skowronek P, Wójcik Ł, Strachecka A. Fat body-multifunctional insect tissue. Insects. 2021;12(6):547.
4. Jia Q, Li S. Mmp-induced fat body cell dissociation promotes pupal development and moderately averts pupal diapause by activating lipid metabolism. Proc Natl Acad Sci USA. 2023;120(1):e2215214120.
5. Liu H, Wang J, Li S. E93 predominantly transduces 20-hydroxyecdysone signaling to induce autophagy and caspase activity in *Drosophila* fat body. Insect Biochem Mol Biol. 2014;45:30–9.
6. Wu W, Luo M, Li K, Dai Y, Yi H, Zhong Y, et al. Cholesterol derivatives induce dephosphorylation of the histone deacetylases Rpd3/HDAC1 to upregulate autophagy. Autophagy. 2021;17(2):512–28.
7. Xie K, Tian L, Guo X, Li K, Li J, Deng X, et al. BmATG5 and BmATG6 mediate apoptosis following autophagy induced by 20-hydroxyecdysone or starvation. Autophagy. 2016;12(2):381–96.
8. Andersen DS, Colombani J, Léopold P. Coordination of organ growth: principles and outstanding questions from the world of insects. Trends Cell Biol. 2013;23(7):336–44.
9. Donoughe S, Nakamura T, Ewen-Campen B, Green DA 2nd, Henderson L, Extavour CG. BMP signaling is required for the generation of primordial germ cells in an insect. Proc Natl Acad Sci U S A. 2014;111(11):4133–8.
10. Johnston LA, Edgar BA. Wingless and Notch regulate cell-cycle arrest in the developing *Drosophila* wing. Nature. 1998;394(6688):82–4.
11. Katsuyama T, Comoglio F, Seimiya M, Cabuy E, Paro R. During *Drosophila* disc regeneration, JAK/STAT coordinates cell proliferation with Dilp8-mediated developmental delay. Proc Natl Acad Sci U S A. 2015;112(18):E2327-2336.
12. Xiang J, Bandura J, Zhang P, Jin Y, Reuter H, Edgar BA. EGFR-dependent TOR-independent endocycles support *Drosophila* gut epithelial regeneration. Nat Commun. 2017;8:15125.
13. Zhang XS, Wei L, Zhang W, Zhang FX, Li L, Li L, et al. ERK-activated CK-2 triggers blastema formation during appendage regeneration. Sci Adv. 2024;10(12):eadk8331.
14. López-Schier H, St JD. Delta signaling from the germ line controls the proliferation and differentiation of the somatic follicle cells during *Drosophila* oogenesis. Genes Dev. 2001;15(11):1393–405.
15. Roy S, Saha TT, Zou Z, Raikhel AS. Regulatory pathways controlling female insect reproduction. Annu Rev Entomol. 2018;63:489–511.
16. Wu Z, Yang L, He Q, Zhou S. Regulatory mechanisms of vitellogenesis in insects. Front Cell Dev Biol. 2020;8:593613.
17. Santos CG, Humann FC, Hartfelder K. Juvenile hormone signaling in insect oogenesis. Curr Opin Insect Sci. 2019;31:43–8.
18. Charles JP, Iwema T, Epa VC, Takaki K, Rynes J, Jindra M. Ligand-binding properties of a juvenile hormone receptor, methoprene-tolerant. Proc Natl Acad Sci U S A. 2011;108(52):21128–33.
19. Li M, Mead EA, Zhu J. Heterodimer of two bHLH-PAS proteins mediates juvenile hormone-induced gene expression. Proc Natl Acad Sci U S A. 2011;108(2):638–43.
20. Zou Z, Saha TT, Roy S, Shin SW, Backman TW, Girke T, et al. Juvenile hormone and its receptor, methoprene-tolerant, control the dynamics of mosquito gene expression. Proc Natl Acad Sci U S A. 2013;110(24):E2173-2181.
21. Guo W, Wu Z, Song J, Jiang F, Wang Z, Deng S, et al. Juvenile hormone-receptor complex acts on *mcm4* and *mcm7* to promote polyploidy and vitellogenesis in the migratory locust. PLoS Genet. 2014;10(10):e1004702.
22. Wang Z, Yang L, Song J, Kang L, Zhou S. An isoform of Taiman that contains a PRD-repeat motif is indispensable for transducing the vitellogenic juvenile hormone signal in *Locusta migratoria*. Insect Biochem Mol Biol. 2017;82:31–40.
23. Liu P, Fu X, Zhu J. Juvenile hormone-regulated alternative splicing of the *taiman* gene primes the ecdysteroid response in adult mosquitoes. Proc Natl Acad Sci U S A. 2018;115(33):E7738–47.
24. Jing YP, Wen X, Li L, Zhang S, Zhang C, Zhou S. The vitellogenin receptor functionality of the migratory locust depends on its phosphorylation by juvenile hormone. Proc Natl Acad Sci USA. 2021;118(37):e2106908118.
25. Wu Z, Yang L, Li H, Zhou S. Krüppel-homolog 1 exerts anti-metamorphic and vitellogenic functions in insects via phosphorylation-mediated recruitment of specific cofactors. BMC Biol. 2021;19(1):222.
26. Zheng H, Wang N, Yun J, Xu H, Yang J, Zhou S. Juvenile hormone promotes paracellular transport of yolk proteins via remodeling zonula adherens at tricellular junctions in the follicular epithelium. PLoS Genet. 2022;18(6):e1010292.
27. Gao Y, Liu S, Jia Q, Wu L, Yuan D, Li EY, et al. Juvenile hormone membrane signaling phosphorylates USP and thus potentiates 20-hydroxyecdysone action in *Drosophila*. Sci Bull (Beijing). 2022;67(2):186–97.
28. Oberlander H, Leach CE, Shaaya E. Juvenile hormone and juvenile hormone mimics inhibit proliferation in a lepidopteran imaginal disc cell line. J Insect Physiol. 2000;46(3):259–65.
29. Capella IC, Hartfelder K. Juvenile hormone effect on DNA synthesis and apoptosis in caste-specific differentiation of the larval honey bee (*Apis mellifera* L.) ovary. J Insect Physiol. 1998;44(5–6):385–91.
30. Guo Z, Kang S, Sun D, Gong L, Zhou J, Qin J, et al. MAPK-dependent hormonal signaling plasticity contributes to overcoming *Bacillus thuringiensis* toxin action in an insect host. Nat Commun. 2020;11(1):3003.
31. Yang X, Deng S, Wei X, Yang J, Zhao Q, Yin C, et al. MAPK-directed activation of the whitefly transcription factor CREB leads to P450-mediated imidacloprid resistance. Proc Natl Acad Sci U S A. 2020;117(19):10246–53.
32. Mirth CK, Tang HY, Makohon-Moore SC, Salhadar S, Gokhale RH, Warner RD, et al. Juvenile hormone regulates body size and perturbs insulin signaling in *Drosophila*. Proc Natl Acad Sci U S A. 2014;111(19):7018–23.
33. Libbrecht R, Corona M, Wende F, Azevedo DO, Serrão JE, Keller L. Interplay between insulin signaling, juvenile hormone, and vitellogenin regulates maternal effects on polyphenism in ants. Proc Natl Acad Sci U S A. 2013;110(27):11050–5.
34. Song J, Li W, Zhao H, Zhou S. Clustered miR-2, miR-13a, miR-13b and miR-71 coordinately target Notch gene to regulate oogenesis of the migratory locust *Locusta migratoria*. Insect Biochem Mol Biol. 2019;106:39–46.
35. Huang J, Tian L, Peng C, Abdou M, Wen D, Wang Y, et al. DPP-mediated TGFbeta signaling regulates juvenile hormone biosynthesis by activating the expression of juvenile hormone acid methyltransferase. Development. 2011;138(11):2283–91.
36. Korchynskyi O, ten Dijke P. Identification and functional characterization of distinct critically important bone morphogenetic protein-specific response elements in the *Id1* promoter. J Biol Chem. 2002;277(7):4883–91.
37. Vuilleumier R, Lian T, Flibotte S, Khan ZN, Fuchs A, Pyrowolakis G, et al. Retrograde BMP signaling activates neuronal gene expression through widespread deployment of a conserved BMP-responsive cis-regulatory activation element. Nucleic Acids Res. 2019;47(2):679–99.

38. Wu Z, Guo W, Xie Y, Zhou S. Juvenile hormone activates the trranscription of *cell-division-cycle 6* (*Cdc6*) for polyploidy-dependent insect vitellogenesis and oogenesis. J Biol Chem. 2016;291(10):5418–27.
39. Wu Z, Guo W, Yang L, He Q, Zhou S. Juvenile hormone promotes locust fat body cell polyploidization and vitellogenesis by activating the transcription of *Cdk6* and *E2f1*. Insect Biochem Mol Biol. 2018;102:1–10.
40. Wu Z, He Q, Zeng B, Zhou H, Zhou S. Juvenile hormone acts through FoxO to promote Cdc2 and Orc5 transcription for polyploidy-dependent vitellogenesis. Dev. 2020;147(18):dev188813.
41. Guo W, Wu Z, Yang L, Cai Z, Zhao L, Zhou S. Juvenile hormone-dependent Kazal-type serine protease inhibitor Greglin safeguards insect vitellogenesis and egg production. Faseb j. 2019;33(1):917–27.
42. Imamura T, Oshima Y, Hikita A. Regulation of TGF-β family signalling by ubiquitination and deubiquitination. J Biochem. 2013;154(6):481–9.
43. Manchado E, Eguren M, Malumbres M. The anaphase-promoting complex/cyclosome (APC/C): cell-cycle-dependent and -independent functions. Biochem Soc Trans. 2010;38(Pt 1):65–71.
44. Pesin JA, Orr-Weaver TL. Regulation of APC/C activators in mitosis and meiosis. Annu Rev Cell Dev Biol. 2008;24:475–99.
45. Qin L, Guimarães DS, Melesse M, Hall MC. Substrate recognition by the Cdh1 destruction box receptor is a general requirement for APC/C(Cdh1)-mediated proteolysis. J Biol Chem. 2017;292(12):5125–7.
46. Li Y, Yao CF, Xu FJ, Qu YY, Li JT, Lin Y, et al. APC/C(CDH1) synchronizes ribose-5-phosphate levels and DNA synthesis to cell cycle progression. Nat Commun. 2019;10(1):2502.
47. Kraft C, Vodermaier HC, Maurer-Stroh S, Eisenhaber F, Peters JM. The WD40 propeller domain of Cdh1 functions as a destruction box receptor for APC/C substrates. Mol Cell. 2005;18(5):543–53.
48. Stewart S, Fang G. Destruction box-dependent degradation of aurora B is mediated by the anaphase-promoting complex/cyclosome and Cdh1. Cancer Res. 2005;65(19):8730–5.
49. Meng L, Dong R, Mi W, Qin K, Ouyang K, Sun J, et al. The ubiquitin E3 ligase APC/C(Cdc20) mediates mitotic degradation of OGT. J Biol Chem. 2024;300(7): 107448.
50. Li L, Zhou Y, Wang GF, Liao SC, Ke YB, Wu W, et al. Anaphase-promoting complex/cyclosome controls HEC1 stability. Cell Prolif. 2011;44(1):1–9.
51. Cho HJ, Lee EH, Han SH, Chung HJ, Jeong JH, Kwon J, et al. Degradation of human RAP80 is cell cycle regulated by Cdc20 and Cdh1 ubiquitin ligases. Mol Cancer Res. 2012;10(5):615–25.
52. Ren C, Wen Y, Zheng S, Zhao Z, Li EY, Zhao C, et al. Two transcriptional cascades orchestrate cockroach leg regeneration. Cell Rep. 2024;43(3):113889.
53. Sardi J, Bener MB, Simao T, Descoteaux AE, Slepchenko BM, Inaba M. Mad dephosphorylation at the nuclear pore is essential for asymmetric stem cell division. Proc Natl Acad Sci USA. 2021;118(13):e2006786118.
54. Tracy Cai X, Li H, Safyan A, Gawlik J, Pyrowolakis G, Jasper H. AWD regulates timed activation of BMP signaling in intestinal stem cells to maintain tissue homeostasis. Nat Commun. 2019;10(1):2988.
55. Gui J, Huang Y, Montanari M, Toddie-Moore D, Kikushima K, Nix S, et al. Coupling between dynamic 3D tissue architecture and BMP morphogen signaling during *Drosophila* wing morphogenesis. Proc Natl Acad Sci U S A. 2019;116(10):4352–61.
56. Qian W, Guo M, Peng J, Zhao T, Li Z, Yang Y, et al. Decapentaplegic retards lipolysis during metamorphosis in *Bombyx mori* and *Drosophila melanogaster*. Insect Biochem Mol Biol. 2023;155:103928.
57. Ishimaru Y, Tomonari S, Matsuoka Y, Watanabe T, Miyawaki K, Bando T, et al. TGF-β signaling in insects regulates metamorphosis via juvenile hormone biosynthesis. Proc Natl Acad Sci U S A. 2016;113(20):5634–9.
58. Guo X, Wang XF. Signaling cross-talk between TGF-beta/BMP and other pathways. Cell Res. 2009;19(1):71–88.
59. Luo K. Signaling cross talk between TGF-β/Smad and other signaling pathways. Cold Spring Harb Perspect Biol. 2017;9(1):a022137.
60. Raikhel AS, Lea AO. Previtellogenic development and vitellogenin synthesis in the fat body of a mosquito: an ultrastructural and immunocytochemical study. Tissue Cell. 1983;15(2):281–99.
61. Qian W, Li Z, Song W, Zhao T, Wang W, Peng J, et al. A novel transcriptional cascade is involved in Fzr-mediated endoreplication. Nucleic Acids Res. 2020;48(8):4214–29.
62. Qian W, Li H, Zhang X, Tang Y, Yuan D, Huang Z, et al. Fzr regulates silk gland growth by promoting endoreplication and protein synthesis in the silkworm. PLoS Genet. 2023;19(1):e1010602.
63. Cohen E, Allen SR, Sawyer JK, Fox DT. Fizzy-related dictates A cell cycle switch during organ repair and tissue growth responses in the *Drosophila* hindgut. Elife. 2018;7:e38327.
64. Djabrayan NJ, Cruz J, de Miguel C, Franch-Marro X, Casanova J. Specification of differentiated adult progenitors via inhibition of endocycle entry in the *Drosophila* trachea. Cell Rep. 2014;9(3):859–65.
65. Sigrist SJ, Lehner CF. *Drosophila* fizzy-related down-regulates mitotic cyclins and is required for cell proliferation arrest and entry into endocycles. Cell. 1997;90(4):671–81.
66. Wu Z, Zhou S. Locusta migratoria decapentaplegic protein mRNA, complete cds. NCBI GenBank https://www.ncbi.nlm.nih.gov/nuccore/PQ367898.1/ (2025).
67. Wu Z, Zhou S. Locusta migratoria mothers against dpp protein mRNA, complete cds. NCBI GenBank https://www.ncbi.nlm.nih.gov/nuccore/PQ367899.1/ (2025).
68. Wu Z, Zhou S. Locusta migratoria mothers against decapentaplegic 4-like protein mRNA, complete cds. NCBI GenBank https://www.ncbi.nlm.nih.gov/nuccore/PQ367900.1/ (2025).
69. Wu Z, Zhou S. Locusta migratoria G2/mitotic-specific cyclin-B mRNA, complete cds. NCBI GenBank https://www.ncbi.nlm.nih.gov/nuccore/PQ367901.1/ (2025).
70. Wu Z, Zhou S. Locusta migratoria serine/threonine protein kinase mRNA, complete cds. NCBI GenBank https://www.ncbi.nlm.nih.gov/nuccore/PQ367902.1/ (2025).
71. Wu Z, Zhou S. Locusta migratoria fizzy-like protein mRNA, complete cds. NCBI GenBank https://www.ncbi.nlm.nih.gov/nuccore/PQ367903.1/ (2025).
72. RNA sequencing of adult fat bodies in the migratory locust. NCBI Bioproject https://www.ncbi.nlm.nih.gov/bioproject/PRJNA1165726/ (2024).

Publisher's Note